

Enhancing radioisotope identification in gamma spectra via supervised domain adaptation

Peter Lalor^{a,*}

^a*Pacific Northwest National Laboratory, Richland, WA 99352 USA*

Abstract

Machine learning methods in gamma spectroscopy have the potential to provide accurate, real-time classification of unknown radioactive samples. However, obtaining sufficient experimental training data is often prohibitively expensive and time-consuming, and models trained solely on simulated data can struggle to generalize to the unpredictable range of real-world operating scenarios. In this study, we explore how supervised domain adaptation techniques can improve radioisotope identification models by transferring knowledge between different data domains. We begin by pretraining a model for radioisotope identification using data from a synthetic source domain, and then fine-tune it for a new target domain that shares the same label space. Our analysis indicates that fine-tuned models significantly outperform those trained exclusively on source-domain data or solely on target-domain data, particularly in the intermediate data regime ($\approx 10^2$ to 10^5 target training samples). This conclusion is consistent across four different machine learning architectures (MLP, CNN, Transformer, and LSTM). Furthermore, our findings show that fine-tuned Transformers yield a statistically significant improvement in test performance compared to the other architectures. Overall, this study serves as a proof of concept for applying supervised domain adaptation techniques to gamma spectroscopy in scenarios where experimental data is limited.

Keywords: Domain Adaptation, Transfer Learning, Gamma Spectroscopy, Radioisotope Identification

1. Introduction

The gamma emission spectrum of a specific set of radioisotopes can serve as a fingerprint for material identification. The ability to quickly identify the presence, type, and quantity of certain radioisotopes has a wide range of applications in national security, including nuclear forensics, arms control, treaty verification, and counter smuggling. Machine learning is an excellent candidate for gamma spectral analysis due to its ability to efficiently decompose complex spectra. However, obtaining sufficient experimental data to train a machine learning model remains a widespread challenge, as manually labeling a large quantity of experimental spectra is tedious and costly.

*Corresponding author
Email address: peter.lalor@pnl.gov
Telephone: (925) 453-1876

Due to the challenges associated with obtaining a comprehensive experimental dataset, most existing literature heavily leverages synthetic data to train classification models. Still, deploying a model trained on synthetic data to a real-world setting can be risky, since the ability for such models to generalize is inherently limited by the sim-to-real gap. In this analysis, we consider the scenario where we have access to a data-rich source domain and wish to transfer knowledge to perform classification in a data-scarce target domain. This scenario parallels the plausible application in gamma spectroscopy where synthetic data is abundant but access to experimental data is limited. In this study, our contributions include the following:

- We propose a supervised domain adaptation framework that adapts a gamma spectral classifier trained on synthetic source-domain data to a new target domain. Our classifier performs multi-label proportion estimation on spectra containing mixtures of up to 14 different radioisotopes.
- We evaluate our framework across four machine learning architectures (MLPs, CNNs, Transformers, and LSTMs), examining model performance over a wide range of target-domain dataset sizes.
- We provide statistical evidence using Wilcoxon signed-rank tests that (i) fine-tuning pretrained models improves performance compared to models trained solely on source-domain data or target-domain data, and (ii) fine-tuned Transformer architectures consistently outperform alternative models.

Obtaining a suitable experimental dataset was prohibitively challenging for this research. Since the primary goal of this study is to benchmark the effectiveness of domain adaptation techniques, we instead use a Geant4 Monte Carlo simulated dataset as the target domain for this analysis [1]. For the source domain, we generated spectra using GADRAS, which is a fast, deterministic tool for synthetically calculating gamma-ray detector responses [2]. While the results of this analysis do not guarantee that these methods would extend to experimental data, this study serves as a proof of concept to adapt a gamma spectral classifier from one data domain to another via supervised domain adaptation.

2. Background

As radioactive material decays, gamma rays are emitted with energies specific to particular decay pathways of the present radioisotopes [3]. The measurement of these gammas yields a gamma spectrum, which is a histogram of detected gamma energies over a measurement period. Traditional techniques for gamma spectral analysis search for peaks in the measured gamma energy spectrum that can then be mapped to specific decay energies of a radioisotope [4, 5, 6]. These methods typically include numerous time-consuming preprocessing steps and require close monitoring by an expert spectroscopist [7, 8, 9]. Furthermore, classical approaches struggle in the presence of thick shielding or when the spectrum contains many overlapping material signatures.

Machine learning presents a promising alternative for improving the speed and accuracy of radioisotope identification using gamma spectroscopy [10, 11, 12, 13, 14, 15, 16, 17]. However, as previously discussed,

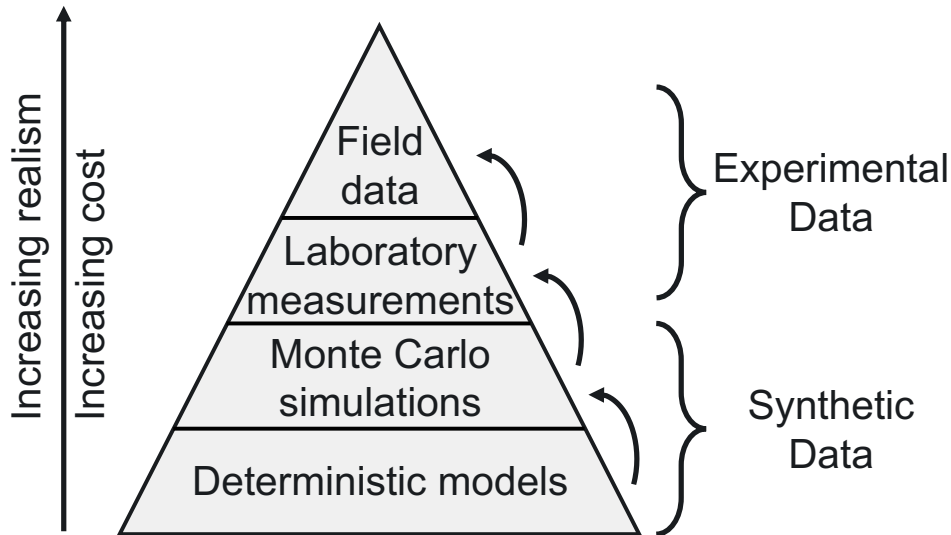


Figure 1: Depiction of a data hierarchy in the field of gamma spectroscopy. Lower levels on the data hierarchy indicate synthetic data, which is cheap and widely available. Higher levels indicate experimental data, which is much more costly but also more realistic for an experimental application. While most existing literature trains machine learning models using data entirely from a single level, we propose leveraging transfer learning techniques (indicated using arrows) to incorporate data across multiple levels.

models trained solely on synthetic data will experience performance degradation when applied to experimental data due to a variety of unpredictable nuances in a real-world setting. We illustrate the concept of a data hierarchy in Fig. 1, whereby lower levels of data are cheaper and more abundant, but also less representative of a typical operational scenario compared to higher levels. Most prior machine learning studies in the field train a spectral classifier using data entirely from a single level (i.e., training a model using exclusively synthetic data or exclusively experimental data). That said, it may be possible to leverage transfer learning techniques to incorporate separate datasets spanning multiple levels of the data hierarchy (represented in Fig. 1 using arrows). In this study, we analyze the extent to which supervised domain adaptation can enhance the capability to perform radioisotope identification in a target domain where data might be limited.

3. Methodology

3.1. Dataset Curation

In this analysis, we simulated a dataset of gamma spectra using both GADRAS (source domain) and Geant4 (target domain). In Geant4, we simulated the gamma emission spectra of 55 individual radioisotopes by uniformly dissolving each isotope in a scintillation cocktail. A high-purity germanium (HPGe) detector was placed one meter from the source, and the energy of all incoming gamma rays was recorded and binned to create a gamma spectrum. The simulations were repeated using a mix of different scintillation cocktails and HPGe detector models in order to capture additional variance which may be present in a realistic environment. We leveraged the G4ARES simulation framework to improve estimations of gamma cascade

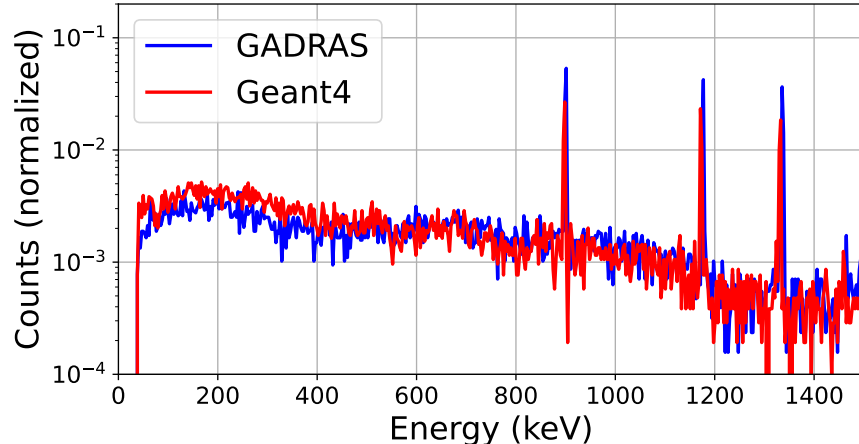


Figure 2: Example training spectra containing mixtures of cobalt-60 and yttrium-88, simulated using GADRAS (blue) and Geant4 (red) with added background and Poisson noise. Characteristic energy peaks at 898 keV (yttrium-88) and 1173 keV and 1333 keV (cobalt-60) are clearly visible in both spectra. Although the overall spectral shapes are similar, minor variations in simulation configurations (e.g., detector properties, energy calibration, and scattering) introduce subtle inter-domain discrepancies. These discrepancies degrade the performance of machine learning models trained in the source domain when tested in the target domain.

summing corrections [18]. In post-processing, we applied a low-energy cutoff and performed Gaussian energy broadening over each spectrum. Furthermore, we introduced slight variations to energy calibration and detector resolution between different detector setups. Once these template spectra were simulated, we created mixed spectra by arbitrarily summing up to 14 individual spectra with random proportions. Our choice to include multiple isotopes per spectrum captures the common scenario in which several radioisotopes are simultaneously present in a material sample. We subsequently added background (cosmic, potassium-40, radium-226, and thorium-232) and Poisson noise, and finally ℓ_1 -normalized the spectra by dividing by the total counts. We synthesized a total of 10^6 training spectra, along with separate holdout sets for validation and testing. To clarify, we did not use the entire dataset for model training. Instead, we trained on data subsets of varying sizes to compare the performance of different models (with and without pretraining) as a function of dataset size.

We followed a similar sequence of steps for generating GADRAS data, first simulating 55 template spectra using a 95% efficiency HPGe detector. The spectra were then mixed, background-added, Poisson resampled, and ℓ_1 -normalized to produce a total of 10^6 training spectra, performed using the PyRIID SeedMixer and StaticSynthesizer classes [19]. We downsampled the spectra to 512 uniform energy bins spanning from 0 keV to 1500 keV in order to speed up runtime and improve memory efficiency. An example gamma spectrum containing a mixture of cobalt-60 and yttrium-88 is shown in Fig. 2 for both the GADRAS and the Geant4 simulations.

3.2. Model training and testing

The downstream task of this study is to perform multi-label proportion estimation. For a given gamma spectrum, up to 14 of the 55 total radioisotope classes may be present, and the presence of each isotope is represented as a proportion between 0 and 1. Note that, unlike traditional classification, our task is to estimate the proportional contributions of each radioisotope (which sum to unity). For this reason, we chose a softmax activation function and a cross-entropy loss function, where we interpret the output of the softmax function as the predicted proportion of the associated radioisotope. Prior literature also considers a sparsemax loss and activation function, which we found yielded nearly identical results [17, 20].

We consider four different machine learning architectures for this analysis: multilayer perceptrons (MLPs), convolutional neural networks (CNNs), Transformers, and long short-term memory networks (LSTMs). MLPs and CNNs are commonly used in prior literature on gamma spectroscopy and serve as simple and effective benchmarks. Transformers and LSTMs are substantially less common in existing literature and are included to provide a comparison using more advanced architectures. For the Transformer and LSTM models, we reshaped each 512-bin spectrum into a matrix of dimensions $\left(\left\lfloor \frac{512}{p} \right\rfloor, p\right)$, where p is a hyperparameter we refer to as the patch size. This approach, inspired by techniques in computer vision [21], allows the models to capture local spectral features more effectively than treating the spectrum as a length 512 sequence of feature dimension 1. All hyperparameters across the different models were optimized using a randomized search with performance-based pruning. Furthermore, training across all architectures was resource-normalized by fixing the total training time. For a detailed discussion of the hyperparameter search methodology and results, see Section Appendix A.1 and Table A.2.

For each architecture, we trained three classes of models using the datasets generated in Section 3.1. The first class was a single model simply trained on the entire source domain (GADRAS) dataset. The second class of models were trained solely on the target-domain (Geant4) data. Within this class, we trained 19 different models, each using a random subset of the Geant4 training data with subset sizes ranging in powers of two from 2^1 to 2^{19} . The third class of models were pretrained using the source-domain dataset, and subsequently fine-tuned using the target-domain data. During the domain adaptation step, we evaluated different fine-tuning strategies. The simplest technique is to continue training all weights in the network on the new dataset using a smaller learning rate. A commonly used alternative approach is to freeze early layers within the network and only fine-tune the output layer(s), thereby preserving high-level features while avoiding catastrophic forgetting. Conversely, prior domain adaptation research suggests that freezing the output layers while fine-tuning only the early layers yields better performance, as the initial layers capture domain-specific features more effectively than the later layers [22]. In our analysis, we incorporated the decision of which (if any) layers to freeze as part of our hyperparameter search. We found that, across all architectures, freezing the output layer yielded validation scores that were comparable or better than those obtained by fine-tuning all layers or only early layers. Notably, within the Transformer architecture, we observed further improvements when additional layers following the final multi-head attention block were

frozen.

4. Analysis

4.1. Defining an evaluation metric

Choosing an evaluation metric for multi-label proportion estimation is less intuitive than for traditional classification problems. In this analysis, we define the absolute proportion error (APE) score, computed by rescaling the mean absolute error to yield a value between 0 and 1. Explicitly,

$$\text{APE score} := 1 - \frac{1}{2N} \sum_{i=1}^N \sum_{j=1}^M |y_{\text{pred},i,j} - y_{\text{true},i,j}| \quad (1)$$

$$\sum_{j=1}^M y_{\text{pred},i,j} = 1, \quad \sum_{j=1}^M y_{\text{true},i,j} = 1.$$

In Eq. 1, N is the number of spectra in the testing dataset, $M = 55$ is the number of radioisotope classes, and y_{pred} and y_{true} are $N \times M$ matrices of the predicted and true proportion labels, respectively. An APE score of 1 indicates perfect agreement between the predicted and true isotope proportions, while a score of 0 reflects maximal deviation. This evaluation metric provides a convenient way to compare how precisely different models predict the fractional composition of each mixed source.

4.2. Comparing model performance

In Fig. 3, we calculate the APE score for each of the three classes of models as a function of the size of the Geant4 training dataset. The models that were only trained on Geant4 data (red error bars) perform especially poorly in the limited data regime ($\lesssim 10^2$ spectra). In the high data regime ($\gtrsim 10^5$ spectra), the models trained on Geant4 data outperform the GADRAS-only model (dashed blue line), highlighting the clear gap between the source domain and the target domain. In all cases, the models that were pretrained on GADRAS and fine-tuned using Geant4 (magenta error bars) yielded APE scores that matched or exceeded those of the GADRAS-only or Geant4-only models. As we would expect, the APE scores of the fine-tuned models approach those of the GADRAS-only model for low amounts of Geant4 data, and similarly approach those of the Geant4-only models for high amounts of Geant4 data. Importantly, in the intermediate domain ($\approx 10^2$ to 10^5 spectra), the fine-tuned models show substantially improved APE scores compared to both the GADRAS-only and Geant4-only models. We quantitatively summarize these results in Table 1, where we explicitly record the APE scores using an intermediate dataset size of 8192 Geant4 samples. For this dataset size, we observe that the models pretrained with GADRAS and fine-tuned using the Geant4 samples substantially outperforms the GADRAS-only and Geant4-only models across all architectures,

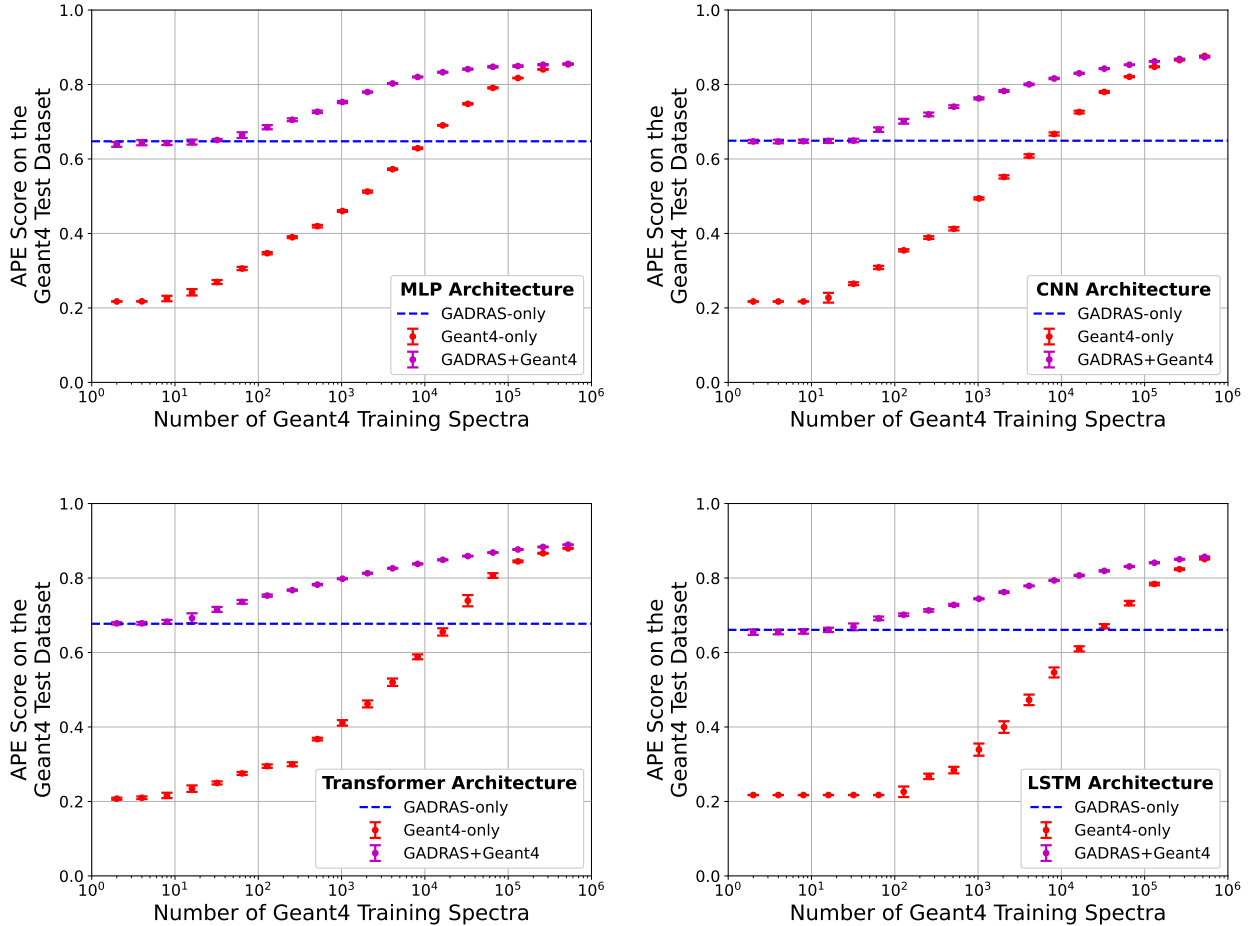


Figure 3: Calculating the APE score (Eq. 1) on the Geant4 test dataset as a function of the Geant4 training dataset size using different model classes and architectures. The red error bars depict models that were trained from scratch using Geant4 data, the dashed blue line depicts a model that was trained using only GADRAS data, and the magenta error bars depict models that were pretrained using GADRAS data and then fine-tuned using Geant4 data. Results are shown using four different architectures: MLPs (top left), CNNs (top right), Transformers (bottom left), and LSTMs (bottom right). The width of each error bar represents the sample standard deviation across 10 repeated trials with randomly drawn Geant4 training samples and different random weight initializations. In all cases, the fine-tuned models yield either comparable or superior APE scores to both the GADRAS-only models and the Geant4-only models.

4.3. Hypothesis testing

To support the conclusions of the previous section, we provide a statistical analysis of the calculated APE scores using a series of one-sided Wilcoxon signed-rank tests. We employ a Wilcoxon signed-rank test because the distribution of APE scores was not assumed to be normal, and we use a one-sided test since we hypothesize that fine-tuning will lead to a strictly larger APE score. For these tests, the null hypothesis states that the difference in APE scores between the fine-tuned models and the baseline models (Geant4-only or GADRAS-only) is nonpositive, and we use a significance threshold of $\alpha = 0.01$.

For each dataset size, we performed 10 repeated trials by retraining each architecture with different initial

Table 1: APE scores (Eq. 1) of the three model classes using different architectures, evaluated on the Geant4 test dataset. Here, we consider an intermediate dataset size of 8192 Geant4 spectra. Uncertainties are calculated as the sample standard deviation of the computed APE scores across 10 repeated trials. In all cases, the models that were pretrained using GADRAS and fine-tuned using the Geant4 spectra yield the best APE scores.

Model Architecture	GADRAS-only model APE score	Geant4-only model APE score	GADRAS+Geant4 model APE score
MLP	0.647 ± 0.001	0.629 ± 0.002	0.820 ± 0.001
CNN	0.649 ± 0.002	0.667 ± 0.004	0.816 ± 0.002
Transformer	0.677 ± 0.004	0.588 ± 0.007	0.838 ± 0.001
LSTM	0.661 ± 0.003	0.546 ± 0.013	0.794 ± 0.001

configurations. We ensured the trials were paired by using the same subset of Geant4 data and identical seed configurations when training both the baseline model (Geant4-only or GADRAS-only) and the fine-tuned model. Specifically, when comparing fine-tuned models to Geant4-only baselines, we randomly selected a subset of the Geant4 dataset for each trial, trained the baseline model, and then fine-tuned a pretrained model on the same subset. Similarly, when comparing fine-tuned models to GADRAS-only baselines, we used the GADRAS model initialization for fine-tuning. We then tested whether the median difference in APE scores (fine-tuned minus baseline) was greater than zero. We plot the calculated p -values of these hypothesis tests along with the median difference in APE scores in Fig. 4 for each model architecture. We also present these results in tabular form in Table A.3. Overall, we conclude a statistically significant improvement to APE score after fine-tuning for most of the trials examined in this study.

We conducted a similar set of hypothesis tests to compare the relative performance of different model architectures. Specifically, for each pair of architectures in $\{\text{MLP, CNN, Transformer, LSTM}\}$, we tested the null hypothesis that the median difference in APE scores of the fine-tuned models on the Geant4 test dataset across trials was zero using a two-sided Wilcoxon signed-rank test. In these experiments, we employ a two-sided test because we do not assume a priori that any given architecture will outperform another. As in the previous example, we treated each set of samples within a trial as paired, since the same Geant4 training subsets were used for both models being compared. The results of these comparisons are presented in Fig. 5, and explicitly recorded in Table A.4. Overall, the fine-tuned Transformer architectures provide a statistically significant improvement to APE score compared to other architectures across all hypothesis tests conducted in this study.

5. Conclusion

In this study, we present a supervised domain adaptation framework for enhancing radioisotope identification in gamma spectra in a target domain where labeled data may be limited. We pretrain a model using a synthetic dataset simulated with GADRAS, and subsequently fine-tune the model to perform multi-label

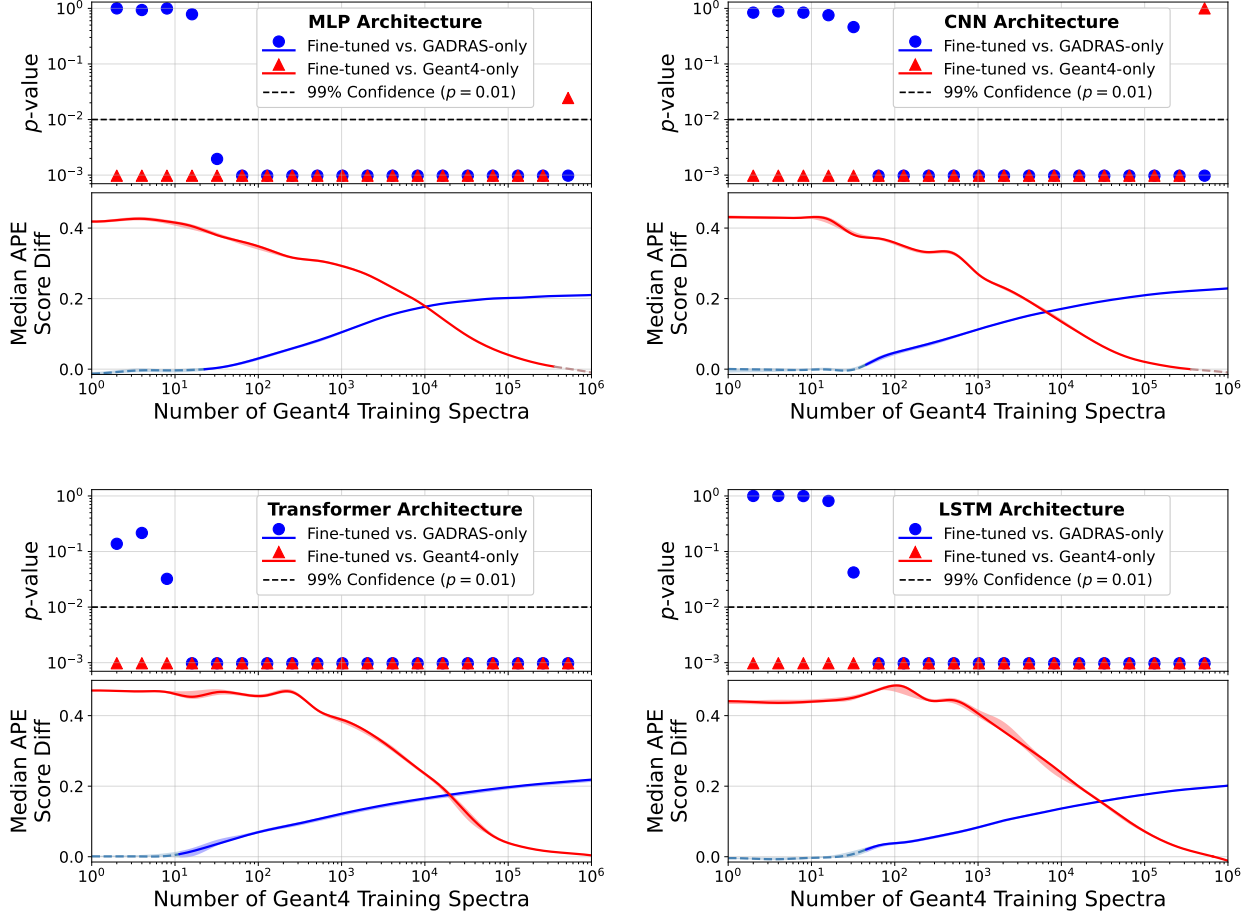


Figure 4: Within each subfigure, the upper plot shows the calculated p -values from a one-sided Wilcoxon signed-rank test comparing the APE scores of fine-tuned models to GADRAS-only models (blue circles) and Geant4-only models (red triangles) as a function of Geant4 training dataset size. Each point represents the p -value from one set of repeated trials, indicating whether fine-tuning yields a statistically significant improvement to APE score compared to the baseline models. The lower plot within each subfigure shows the median difference in calculated APE scores across each set of trials (red lines: fine-tuned minus GADRAS-only; blue lines: fine-tuned minus Geant4-only). We use dashed lines rendered in a muted color to indicate trials where we cannot reject the null hypothesis, and include a 95% confidence band calculated using the percentile bootstrap method. The four subfigures represent repeated experiments using different architectures: MLPs (top left), CNNs (top right), Transformers (bottom left), and LSTMs (bottom right). In most scenarios, we reject the null hypothesis of no improvement with over 99% confidence, with the exception of (i) fine-tuned versus GADRAS-only at smaller training sizes (≤ 32 spectra for CNNs and LSTMs, ≤ 16 spectra for MLPs, ≤ 8 spectra for Transformers), and (ii) fine-tuned versus Geant4-only for larger training sizes ($\gtrsim 5 \cdot 10^5$ spectra) for MLPs and CNNs. For a quantitative summary of these results, see Table A.3.

proportion estimation in a target domain simulated in Geant4. We evaluate four different architectures (MLP, CNN, Transformer, LSTM) and find that fine-tuning yields consistent improvements in APE score, especially in the intermediate data regime ($\approx 10^2$ to 10^5 target training samples). Moreover, statistical analysis indicates that fine-tuned Transformer models outperform other architectures. These results present a promising path forward for applying domain adaptation to gamma spectroscopy, particularly in scenarios where limited experimental data is available. Future work should focus on validating this framework on

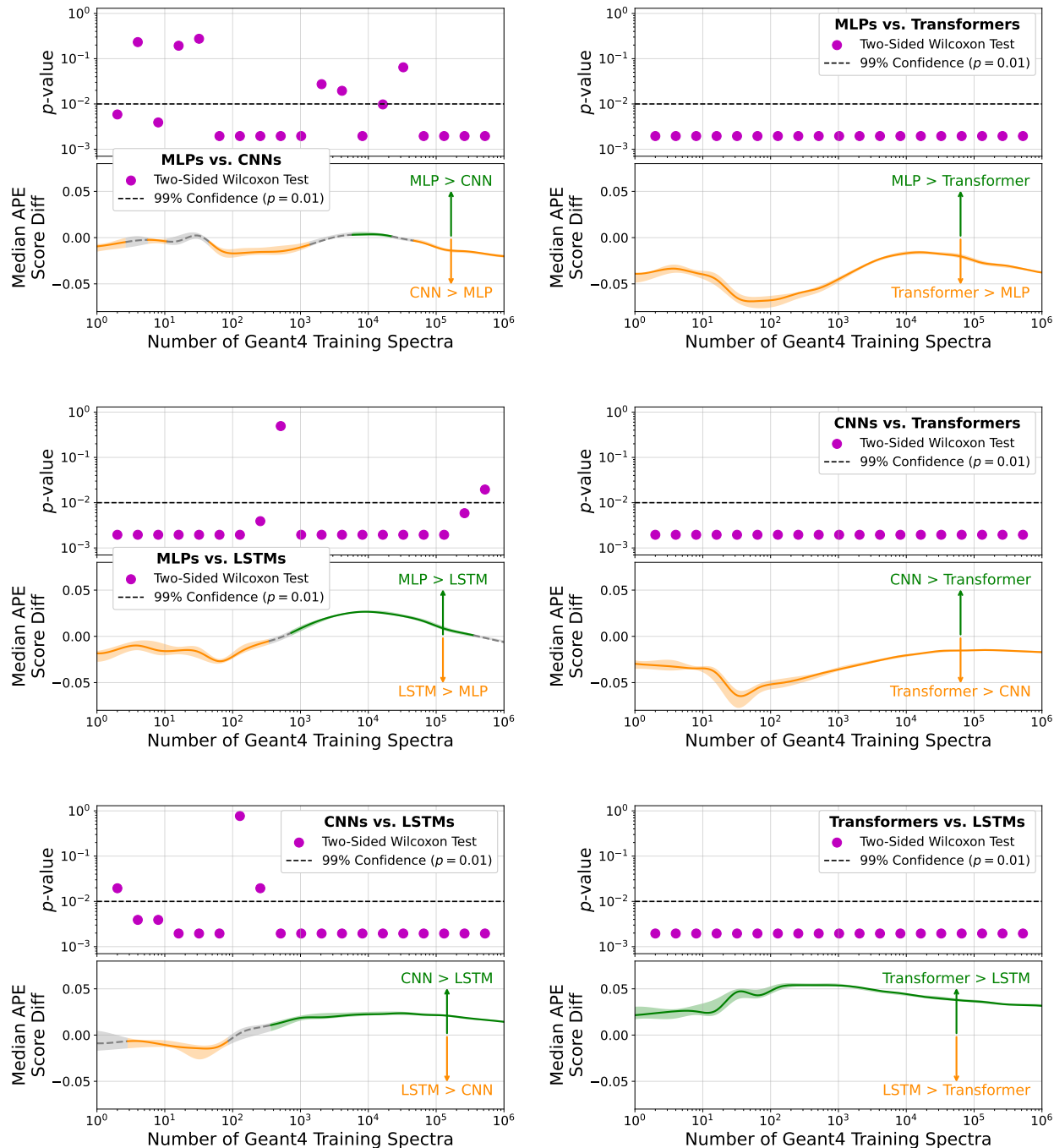


Figure 5: Within each subfigure, the upper plot shows the calculated p -values from a two-sided Wilcoxon signed-rank test comparing the APE scores from fine-tuned models of different architectures: MLPs versus CNNs (top left), MLPs versus Transformers (top right), MLPs versus LSTMs (center left), CNNs versus Transformers (center right), CNNs versus LSTMs (bottom left), and Transformers versus LSTMs (bottom right). Each magenta point represents the p -value from one set of repeated trials, indicating whether there is a statistically significant difference in APE score between the two model architectures after fine-tuning. The lower plot within each subfigure shows the median difference in calculated APE scores across each set of trials. The line is color coded based on its sign (green \implies the first model yields better APE scores; orange \implies the second model yields better APE scores; gray \implies we cannot reject the null hypothesis) and we include a 95% confidence band calculated using the percentile bootstrap method. We observe that the Transformer architectures provide a statistically significant improvement to APE score compared to other architectures. For a quantitative summary of these results, see Table A.4.

experimental datasets to further assess its real-world applicability, while also exploring alternative methods for domain adaptation such as retrieval-augmented generation or optimal transport.

6. Acknowledgements

This research was supported by the Laboratory Directed Research and Development Program at Pacific Northwest National Laboratory, a multiprogram national laboratory operated by Battelle for the U.S. Department of Energy under contract DE-AC05-76RLO1830. Peter Lalor is grateful for the support of the Linus Pauling Distinguished Postdoctoral Fellowship. The authors would like to acknowledge Alex Hagen, Tyler Morrow, and Brian Archambault for their useful suggestions and feedback. The authors declare no conflict of interest.

References

- [1] J. Allison, K. Amako, J. Apostolakis, P. Arce, M. Asai, T. Aso, E. Bagli, A. Bagulya, S. Banerjee, G. Barrand, et al., Recent developments in geant4, Nuclear Instruments and Methods in Physics Research Section A: Accelerators, Spectrometers, Detectors and Associated Equipment 835 (2016) 186–225. doi:10.1016/j.nima.2016.06.125.
URL <https://www.sciencedirect.com/science/article/pii/S0168900216306957>
- [2] D. J. Mitchell, L. Harding, G. G. Thoreson, S. M. Horne, GADRAS detector response function., Tech. rep., Sandia National Lab.(SNL-NM), Albuquerque, NM (United States) (2014).
- [3] G. F. Knoll, Radiation detection and measurement, John Wiley & Sons, 2010.
- [4] T. E. Sampson, Plutonium isotopic analysis using pc / fram (2007).
URL <https://api.semanticscholar.org/CorpusID:34732969>
- [5] Canberra Industries, Inc., Genie™2000 Spectroscopy Software, Canberra Industries, Inc., Meriden, CT, USA, operations, Version 3.1, Document No. 9233652F (2006).
URL <http://www.canberra.com>
- [6] Los Alamos National Laboratory, PeakEasy Software, Los Alamos National Laboratory, version 5.21. (2023).
URL <https://peakeasy.lanl.gov>
- [7] E. Leonard, USDOE, Peak map, version 1.2 (10 2020). doi:10.11578/dc.20201102.3.
URL <https://www.osti.gov/biblio/1696965>
- [8] M. Darweesh, S. Shawky, Study on the performance of different uranium isotopic codes used in nuclear safeguards activities, Heliyon 5 (4) (2019) e01470. doi:10.1016/j.heliyon.2019.e01470.
URL <https://www.sciencedirect.com/science/article/pii/S2405844018368932>
- [9] M. Croce, D. Becker, K. Koehler, J. Ullom, Improved nondestructive isotopic analysis with practical microcalorimeter gamma spectrometers (04 2021). doi:10.48550/arXiv.2104.03376.
- [10] E. T. Moore, J. L. Turk, W. P. Ford, N. J. Hoteling, L. S. McLean, Transfer learning in automated gamma spectral identification (2020). arXiv:2003.10524.
URL <https://arxiv.org/abs/2003.10524>
- [11] D. Liang, P. Gong, X. Tang, P. Wang, L. Gao, Z. Wang, R. Zhang, Rapid nuclide identification algorithm based on convolutional neural network, Annals of Nuclear Energy 133 (2019) 483–490. doi:10.1016/j.anucene.2019.05.051.
URL <https://www.sciencedirect.com/science/article/pii/S0306454919303044>
- [12] A. Khatiwada, M. Klasky, M. Lombardi, J. Matheny, A. Mohan, Machine learning technique for isotopic determination of radioisotopes using hpge gamma-ray spectra, Nuclear Instruments and Methods in Physics Research Section A: Accelerators, Spectrometers, Detectors and Associated Equipment 1054 (2023) 168409. doi:10.1016/j.nima.2023.168409.
URL <https://www.sciencedirect.com/science/article/pii/S0168900223003996>

- [13] M. Kamuda, J. Zhao, K. Huff, A comparison of machine learning methods for automated gamma-ray spectroscopy, *Nuclear Instruments and Methods in Physics Research Section A: Accelerators, Spectrometers, Detectors and Associated Equipment* 954 (2020) 161385, symposium on Radiation Measurements and Applications XVII. doi:10.1016/j.nima.2018.10.063.
URL <https://www.sciencedirect.com/science/article/pii/S0168900218313779>
- [14] K. J. Bilton, T. H. Y. Joshi, M. S. Bandstra, J. C. Curtis, D. Hellfeld, K. Vetter, Neural network approaches for mobile spectroscopic gamma-ray source detection, *Journal of Nuclear Engineering* 2 (2) (2021) 190–206. doi:10.3390/jne2020018.
URL <https://www.mdpi.com/2673-4362/2/2/18>
- [15] T. Grimes, B. A. Wilson, R. W. Gladen, J. Dermigny, B. B. Cipiti, N. Shoman, Neural assessment of non-destructive assay for material accountancy, *Institute of Nuclear Materials Management (INMM)* (2021).
- [16] A. Van Omen, T. Morrow, A semi-supervised learning method to produce explainable radioisotope proportion estimates for nai-based synthetic and measured gamma spectra (2 2024). doi:10.2172/2335904.
URL <https://www.osti.gov/biblio/2335904>
- [17] A. Van Omen, T. Morrow, C. Scott, E. Leonard, Multilabel proportion prediction and out-of-distribution detection on gamma spectra of short-lived fission products, *Annals of Nuclear Energy* 208 (2024) 110777. doi:10.1016/j.anucene.2024.110777.
URL <https://www.sciencedirect.com/science/article/pii/S0306454924004407>
- [18] B. Archambault, B. Pierson, B. Loer, G4ares-geant4 advanced radio-emission simulation framework, available from <https://gitlab.pnnl.gov/ares/g4ares> [accessed November 20, 2024] (2023).
- [19] T. Morrow, N. Price, T. McGuire, Pyriid v.2.0.0, [Computer Software] (apr 2021). doi:10.11578/dc.20221017.2.
URL <https://doi.org/10.11578/dc.20221017.2>
- [20] A. Martins, R. Astudillo, From softmax to sparsemax: A sparse model of attention and multi-label classification, in: *International conference on machine learning*, PMLR, 2016, pp. 1614–1623.
- [21] A. Dosovitskiy, L. Beyer, A. Kolesnikov, D. Weissenborn, X. Zhai, T. Unterthiner, M. Dehghani, M. Minderer, G. Heigold, S. Gelly, J. Uszkoreit, N. Houlsby, An image is worth 16x16 words: Transformers for image recognition at scale (2021). arXiv:2010.11929.
URL <https://arxiv.org/abs/2010.11929>
- [22] B. Shirokikh, I. Zakazov, A. Chernyavskiy, I. Fedulova, M. Belyaev, First u-net layers contain more domain specific information than the last ones (2020). arXiv:2008.07357.
URL <https://arxiv.org/abs/2008.07357>

Appendix A. Supplementary Materials

Appendix A.1. Hyperparameter search

For each architecture, we conducted a random search over 500 hyperparameter configurations. Each model was trained for 18 minutes on an NVIDIA Tesla V100 GPU with 32 GB of memory, with the number of epochs adjusted dynamically to maintain a consistent overall training time. Underperforming configurations were pruned early, and an early stopping criterion was applied to mitigate overfitting. Hyperparameters were ranked by their validation APE scores, and the best-performing model was trained for an additional 72 minutes. We then performed a similar analysis for computing fine-tuning hyperparameters, beginning with a pretrained model that was subsequently fine-tuned on a subset of 8192 spectra from the target training dataset. Table A.2 summarizes the ranges of hyperparameters tested and the selected values for each architecture.

Appendix A.2. p -value tables

In Section 4.3, we performed statistical comparisons of the computed APE scores for different model training strategies and architectures using a series of Wilcoxon signed-rank tests, and present the results in Figs. 4 and 5. We quantitatively summarize these results in Tables A.3 and A.4, where we explicitly record the computed p -values for each series of tests. As noted in Section 4.3, we can reject the null hypothesis (indicated using bold font) in the following notable scenarios: (i) fine-tuned versus Geant4-only models for datasets of size up to 2^{18} spectra (for MLPs and CNNs) or up to 2^{19} spectra (for Transformers and LSTMs), (ii) fine-tuned versus GADRAS-only models for datasets of size at least 2^6 spectra (for CNNs and LSTMs), at least 2^5 spectra (for MLPs), or at least 2^4 spectra (for Transformers), and (iii) fine-tuned Transformer models versus all other fine-tuned architectures for all dataset sizes.

Appendix A.3. Loss curve

Another takeaway of this research is that, after pretraining a model, the subsequent fine-tuning step is substantially faster than training a model from scratch on the same target-domain dataset size. This result is highlighted in Fig. A.6, where we demonstrate that using an MLP architecture, a GADRAS-pretrained model requires nearly an order of magnitude fewer epochs to converge compared to a model trained from scratch using only Geant4 data. In this comparison, we use the same batch size for both models to ensure the same number of gradient updates per epoch. This result demonstrates that using pretrained models can substantially reduce the computational burden of training models, particularly if a model needs to be frequently retrained. This finding is especially pertinent if pretrained models become publicly available in the field of gamma spectroscopy, much like they are in other research domains.

Table A.2: Hyperparameter optimization summary for MLP, CNN, Transformer, and LSTM architectures. The table details the search spaces and best-performing hyperparameter values obtained via a randomized search with performance-based pruning.

Architecture	Parameter	Search Space	Best run
MLP	Batch Size	{32, 512}	256
	Batch Size (fine-tuning)	{32, 128}	64
	Learning Rate	{2e-3, 1e-5}	7e-4
	Learning Rate (fine-tuning)	{7e-4, 7e-6}	3e-4
	Dropout	{0.0, 0.4}	0.0
	Num Dense Layers	{1, 5}	2
	Dense1 Hidden Units	{256, 16384}	4096
	Dense2 Hidden Units	{128, 8192}	2048
	Frozen Layers (fine-tuning)	{none, all}	none
CNN	Batch Size	{32, 512}	512
	Batch Size (fine-tuning)	{32, 128}	32
	Learning Rate	{2e-3, 1e-5}	1e-3
	Learning Rate (fine-tuning)	{1e-3, 1e-5}	7e-4
	Dropout	{0.0, 0.4}	0.0
	Num Convolutional Layers	{1, 5}	2
	Conv1 Filters	{16, 64}	16
	Conv2 Filters	{32, 128}	64
	Conv1 Kernel Size	{5, 7}	5
	Conv2 Kernel Size	{3, 5}	3
	Final Dense Units	{512, 8192}	2048
	Frozen Layers (fine-tuning)	{none, all}	output layer
	Transformer	Batch Size	{32, 512}
Batch Size (fine-tuning)		{32, 128}	32
Learning Rate		{2e-3, 1e-5}	5e-4
Learning Rate (fine-tuning)		{1e-3, 5e-5}	2e-4
Dropout		{0.0, 0.4}	0.0
Embedding Dimension		{32, 512}	64
Number of Heads		{4, 32}	16
FF Dimension		{512, 4096}	4096
Num Attention Blocks		{1, 3}	3
Patch Size		{4, 32}	32
Frozen Layers (fine-tuning)		{none, all}	final feed-forward subnetwork through output layer
LSTM	Batch Size	{32, 512}	128
	Batch Size (fine-tuning)	{32, 128}	32
	Learning Rate	{2e-3, 1e-5}	1e-3
	Learning Rate (fine-tuning)	{1e-3, 1e-5}	7e-4
	Dropout	{0.0, 0.4}	0.0
	Num LSTM Layers	{1, 3}	1
	Number of Hidden Units	{128, 2048}	1024
	Patch Size	{4, 64}	64
	Bidirectional LSTM	{true, false}	true
	Frozen Layers (fine-tuning)	{none, all}	output layer

Table A.3: Calculated p -values using a one-sided Wilcoxon signed-rank test, testing the null hypothesis that the fine-tuned models do not yield any improvement to APE score (Eq. 1) compared to the GADRAS-only or Geant4-only models. We use bold font to indicate scenarios where we can reject the null hypothesis at a significance threshold of $\alpha = 0.01$. For conciseness, we condense all training sizes between 2^6 and 2^{18} to one row, since the calculated p -values for all hypothesis tests in this range yield the same results. For a visual summary of these results, see Fig. 4

Geant4 Dataset Size	MLP p -values		CNN p -values		Transformer p -values		LSTM p -values	
	Fine-tuned vs. Geant4-only	Fine-tuned vs. GADRAS-only	Fine-tuned vs. Geant4-only	Fine-tuned vs. GADRAS-only	Fine-tuned vs. Geant4-only	Fine-tuned vs. GADRAS-only	Fine-tuned vs. Geant4-only	Fine-tuned vs. GADRAS-only
2^1	0.001	0.999	0.001	0.839	0.001	0.138	0.001	1.000
2^2	0.001	0.935	0.001	0.884	0.001	0.216	0.001	1.000
2^3	0.001	0.995	0.001	0.839	0.001	0.032	0.001	0.995
2^4	0.001	0.784	0.001	0.754	0.001	0.001	0.001	0.812
2^5	0.001	0.002	0.001	0.461	0.001	0.001	0.001	0.042
2^6 to 2^{18}	0.001							
2^{19}	0.024	0.001	1.000	0.001	0.001	0.001	0.001	0.001

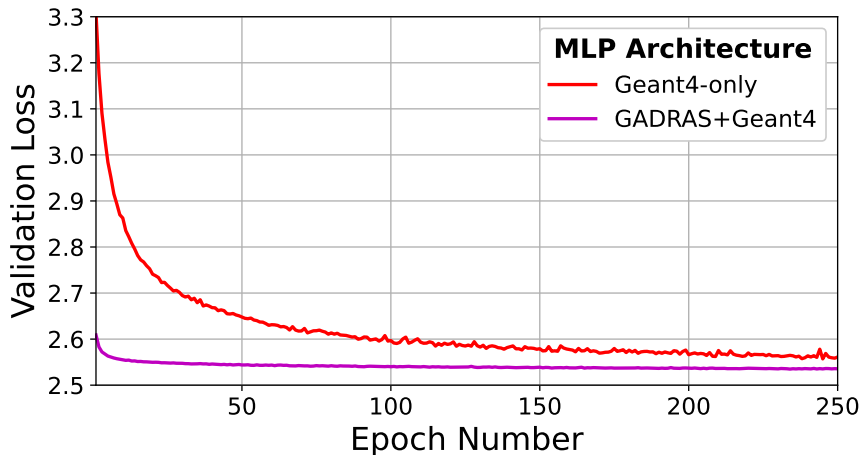


Figure A.6: Comparing the validation cross-entropy loss of a trained-from-scratch MLP to a GADRAS-pretrained MLP as a function of epoch number. We observe that the pretrained model converges substantially faster (≈ 50 epochs) compared to the trained-from-scratch model (≈ 200 epochs).

Table A.4: Calculated p -values using a two-sided Wilcoxon signed-rank test, testing the null hypothesis that there is no difference in APE score (Eq. 1) between different fine-tuned architectures. We use bold font to indicate scenarios where we can reject the null hypothesis at a significance threshold of $\alpha = 0.01$. For a visual summary of these results, see Fig. 5

Geant4 Dataset Size	MLPs vs. CNNs	MLPs vs. Transformers	MLPs vs. LSTMs	CNNs vs. Transformers	CNNs vs. LSTMs	Transformers vs. LSTMs
2^1	0.006	0.002	0.002	0.002	0.020	0.002
2^2	0.232	0.002	0.002	0.002	0.004	0.002
2^3	0.004	0.002	0.002	0.002	0.004	0.002
2^4	0.193	0.002	0.002	0.002	0.002	0.002
2^5	0.275	0.002	0.002	0.002	0.002	0.002
2^6	0.002	0.002	0.002	0.002	0.002	0.002
2^7	0.002	0.002	0.002	0.002	0.770	0.002
2^8	0.002	0.002	0.004	0.002	0.020	0.002
2^9	0.002	0.002	0.492	0.002	0.002	0.002
2^{10}	0.002	0.002	0.002	0.002	0.002	0.002
2^{11}	0.027	0.002	0.002	0.002	0.002	0.002
2^{12}	0.020	0.002	0.002	0.002	0.002	0.002
2^{13}	0.002	0.002	0.002	0.002	0.002	0.002
2^{14}	0.010	0.002	0.002	0.002	0.002	0.002
2^{15}	0.064	0.002	0.002	0.002	0.002	0.002
2^{16}	0.002	0.002	0.002	0.002	0.002	0.002
2^{17}	0.002	0.002	0.002	0.002	0.002	0.002
2^{18}	0.002	0.002	0.006	0.002	0.002	0.002
2^{19}	0.002	0.002	0.020	0.002	0.002	0.002